Biomedical Microdevices (2020) 22: 31
https://doi.org/10.1007/s10544-020-00485-5

Breast Tumor Targeting with PAMAM-PEG-5FU-^{99m}Tc As a New Therapeutic Nanocomplex: *In In-vitro* and *In-vivo* studies

Asghar Narmani[1] · Monire Alsadat Afzali Arani[2] · Javad Mohammadnejad[1] · Ali Zaman Vaziri[3] · Sedigheh Solymani[2] · Kamal Yavari[4] · Farideh Talebi[5] · Simin Janitabar Darzi[4]

Published online: 25 April 2020

Abstract

Dendrimer-based targeted drug delivery, as an innovative polymeric drug-delivery system, is promising for cancer therapy. Folate receptors (FR) are overexpressed in many types of tumor cells, such as breast cell carcinomas, which allow folate-targeted delivery. Therefor polyethylene glycol (PEG) modified-PAMAM G4 dendrimers were functionalized with folic acid (FA), as targeting agent. Then, 5-FU (5-fluorouracil) and ^{99m}Tc (technetium-99 m) as therapeutic agents were respectively loaded and conjugated to previous nano-complex (PEG-PAMAM G4-FA-5FU-^{99m}Tc). The value of drug loading was calculated by TGA analysis (16.97%). Drug release profiles of PEG-PAMAM G4-FA-5FU-^{99m}Tc and PEG-PAMAM G4-FA-5FU were evaluated. The radiochemical purity of PEG-PAMAM G4-FA-5FU-^{99m}Tc and PEG-PAMAM G4-FA-^{99m}Tc was obtained at >95% with excellent *in-vitro* and *in-vivo* stabilities. PEG-PAMAM G4-FA-5FU-^{99m}Tc was synthesized and the stability studies were carried out by the ITLC methods in serum (86.67% and 83.75%) and PBS. Combinational therapy effects of 5-FU and ^{99m}Tc containing nano-complexes were evaluated on 4 T1 (mouse breast cancer) and MDA-MB-231 (human breast adenocarcinoma) cancer cell lines. Excellent uptake values were obtained for FA-decorated nano-complexes on 4 T1 and MDA-MB-231 cell lines. Subsequently, tumor inhibition effects of PEG-PAMAM G4-FA-5FU-^{99m}Tc and PEG-PAMAM G4-FA-5FU were evaluated using the breast tumor-bearing BALB/C mice.

Keywords Breast cancer · PAMAM G4-PEG · Folic acid targeting · 5-FU delivery · ^{99m}Tc

Abbreviations

PEG	polyethylene glycol
PAMAM	polyamidoamine dendrimers G4
FA	Folic acid
5-FU	5fluorouracil
^{99m}Tc	^{99m}Technetium
P-P	polyethylene glycol-polyamidoamine dendrimers G4
P-P-FA	polyethylene glycol-polyamidoamine dendrimers G4-Folic acid
P-P-FA-5FU	polyethylene glycol-polyamidoamine dendrimers G4-Folic acid-5fluorouracil
P - P - F A - 5 F U - Suc-^{99m}Tc	polyethylene glycol-polyamidoamine dendrimers G4-Folic acid-5fluorouracil-Succinimidyl HYNIC-^{99m}Technetium
Suc	Succinimidyl HYNIC
FR	Folic acid receptors
EPR	Enhanced permeability and retention; Dynamic light scattering
TGA	Thermogravimetric analysis
DSC	Differential scanning calorimetry analysis
MTT	3-[4,5-dimethylthiazol-2-yl]-2,5-diphenyl tetrazolium bromide
DMF	Dimethyl formamide and
DMSO	Dimethyl sulfoxide

✉ Javad Mohammadnejad
mohamadnejad@ut.ac.ir

[1] Department of Life Science Engineering, Faculty of New Sciences and Technologies, University of Tehran, Tehran 1439957131, Islamic Republic of Iran

[2] Department of Molecular Medicine, Cancer Biomedical Center, Tehran, Iran

[3] Department of Molecular Genetics, Tehran Medical Science Branch, Islamic Azad University, Tehran, Iran

[4] Department of Nuclear Science and Technology Research Institute, Tehran, Iran

[5] Immunoregulation Research Center, Shahed University, Tehran, Iran

1 Introduction

Nanoparticle-based targeted drug-delivery systems have added a new dimension to the therapeutic approach for the treatment of cancer due to their unique accumulation behavior at the tumor sites (Blanco et al. 2015; Sega and Low 2008; Narmani et al. 2018a). Breast cancer was once considered a frequently-diagnosed deadly form of cancer in women (Ferlay et al. 2013). Chemotherapy plays a major role in cancer treatment, and the scientific advances in chemotherapy over the last several years have led to significant ongoing patient therapy rates (Satsangi et al. 2015). The polyamidoamine dendrimers G4 (PAMAM G4), due to monodispersity, nanosize (1–100 nm) and shape, good biocompatibility, high capacity to surface modification, and functionalization (polyvalency properties of PAMAM G4), good *in-vitro* and *in-vivo* stabilities, excellent pharmacokinetics properties have been good candidates for drug delivery (Agrawal et al. 2007; Narmani et al. 2019a; Yousefi et al. 2020). Polyethylene glycol (PEG) is one of the promising candidates for modifying PAMAM dendrimers to overcome possible cytotoxicity and hemolytic toxicity, increasing biocompatibility, increasing the solubility of both drugs and nanocarriers, decreasing the aggregation of nanoparticles, increasing tumor accumulation by strengthening the enhanced permeability and retention (EPR) effect, and for its good bioavailability (Luong et al. 2016; Amini et al. 2019).

On the other hand, this targeting leads to a decrease in the uptake of the drug by the normal tissue, as many receptors are present in the diseased tissues and cells. It is well known that folate receptors (FR), as the most promising sites for FA moiety, are overexpressed in various human cancer cells, including the breast, ovary, endometrium, kidney, lung, head and neck, brain, and myeloid cancers, even though they are fairly limited in normal cells (Wang et al. 2012; Zheng et al. 2016; Narmani et al. 2018b; Evans et al. 2016). Also, FR has more expression in various inflammatory diseases. FR, with 38–40 KDa in molecular weight, is a glycosylphosphatidylinositol (GPI)-anchored membrane-bound protein that binds itself to folic acid moiety with high affinity and can be internalized into the cytoplasm by endocytosis (Cui et al. 2017). The FR exists in three major forms: FR-α, FR-β, and FR-γ. FR-α is overexpressed in many tumors, such as breast carcinomas. The covalent linkage of folate to γ-carboxyl retains high-affinity FR-binding and agitates the FR overexpression in tumors (Rezvani et al. 2018; Narmani et al. 2019b). The FR-α in a low-pH condition in the endosome vesiculs leads to the release of folic acid from the complex that has been exploited for the delivery of small chemotherapeutic drugs (Satsangi et al. 2015; Sulistio et al. 2011). The site-specific delivery of anti-neoplastic and chemotherapeutic agents may reduce their systemic side effects, resulting in their effective and safe performance. Chemotherapeutical drugs, such as 5-fluorouracil (5FU), azathioperine, cyclophosphamide, methotrexate, doxorubicin, and vincristine, which can be conjugated to PAMAM G4. 5FU, as a chemotherapeutic agent, has been widely used in different solid tumor types, such as cancer of the breast, stomach, liver, and intestine, to name a few. It has been mentioned that 5FU should be specifically dosed once or twice a week as a targeting therapy (Leelakanok et al. 2017). This drug interferes with thymidylate synthesis, and by conversion to fluorodeoxyuridine monophosphate, leads to the inhibition of RNA function and/or the processing and synthesizing of thymidylate and, finally, annihilation of the cell (Gómez-Canela et al. 2017).

Besides, radioisotope ^{99m}Tc has high usage in particle-based radiopharmaceuticals and is currently utilized as a good imaging and therapeutic agent in nuclear medicine, paving the way for practical applications because of its ideal physical properties, suitable dosimetry, and high specific activity. Hydrazinonicotinamide (HYNIC), as a suitable linker, has been conjugated to peptides and proteins for several years (Liu et al. 2001; Torabizadeh et al. 2017; Narmani et al. 2018c). Mostly, some co-ligands, such as tricine or ethylenediaminediaceticacid (EDDA), have been used in ^{99m}Tc labeling of HYNIC conjugates. Co-ligands bring about good stability, high specific radioactivity, higher labeling efficiency, and excellent dendrimer-binding potency of the radiolabels (Guo et al. 2011; Mombini et al. 2019).

In our previous work, we designed and synthesized an FA-PAMAM G4-PEG-5FU-Suc-^{99m}Tc nano-complex as a novel targeted drug-delivery system, and we investigated biodistribution and imaging ability of above-mentioned nano-complex (Narmani et al. 2019a). However, in this work we evaluated drug loading efficiency and drug release behavior of 5-FU in FA-PAMAM G4-PEG-5FU-Suc-^{99m}Tc and FA-PAMAM G4-PEG-5FU nano-complexes. The thermal stability of FA-PAMAM G4-PEG-5FU-Suc-^{99m}Tc nano-complex and its derivate was investigated. Cellular uptake values of FA-decorated FA-PAMAM G4-PEG-5FU-Suc-^{99m}Tc and FA-PAMAM G4-PEG-Suc-^{99m}Tc nano-complexes were determined and compared with each other. Combinational therapy effects of 5-FU and ^{99m}Tc containing nano-complexes were evaluated on 4 T1 (mouse breast cancer) and MDA-MB-231 (human breast adenocarcinoma) cancer cell lines. Then, PEG-PAMAM G4-FA-5FU-Suc-^{99m}Tc and PEG-PAMAM G4-FA-5FU nano-complexes as highly effective delivery systems were intravenously injected in breast tumor-bearing BALB/C mice and tumor growth inhibition and therapeutic ability of 5-FU- and ^{99m}Tc-conjugated nano-complex were evaluated.

2 Experimental details

2.1 Materials and apparatus

MTT (3-[4,5-dimethylthiazol-2-yl]-2,5-diphenyl tetrazolium bromide, CAS Number: 298-93-1), penicillin, streptomycin, and fetal bovine serum (FBS), and cellulose dialysis membranes (molecular weight cut-off, MW = 12,000 Da) were bought from Sigma-Aldrich. Di-tert-butyldicarbonate (Boc) was bought from Flukachamika. Dimethylformamide (DMF) and dimethylsulfoxide (DMSO) were bought from Sigma-Aldrich. The ^{99m}Tc was obtained from a ^{99}Mo/^{99m}Tc generator. C2C12, MDA-MB-231 and 4T1cell lines were bought from the Institute of Pasteur, Iran.

TGA and DSC were implemented by STA 1500, rheometric-scientific. Spectroscopy evaluation was performed via Nanodrop 2000c UV–vis spectrophotometer, Thermo Scientific. Freeze-dry carried out by freeze-vacuum dryer (Freezone 6, USA). Cell viability assay was measured by means of Elisa Reader (SpectraMax M2e, Molecular Devices). Labeling efficiency of ^{99m}Tc was determined by γ-counter (EG& G ORTECH 4001 M).

2.2 *In-vitro* stability of the radio-labeled sample

ITLC was used to assess the *in-vitro* stability of ^{99m}Tc radio-labeled P-P-FA and P-P-FA-5FU in serum and PBS. 150 μl (200 μCi) of the P-P-FA-Suc-^{99m}Tc and P-P-F-A-5FU-Suc-^{99m}Tc complex was added to 2 ml of fresh human serum and 1 ml of PBS separately and was incubated at 37 °C for different lengths of time (1, 3, and 24 h). 1 × 10.5 cm strips of Whatman No. 1 paper were used to check each sample at different lengths of time (Guo et al. 2011; Song et al. 2017). Finally, each strip was read using the γ-counter (Guo et al. 2011).

2.3 Drug loading efficiency and drug-release studies

5-FU Loading efficiency of synthetic nano-complex was calculated by absence or shifting of endothermic peaks by means of thermogravimetric analysis (TGA). Furthermore, the thermal stability and physical state of P-P-FA-5FU and P-P-FA-Suc-5FU nanocomplexes were evaluated thermal gravimetric spectroscopies. On the other hand, the profiles of 5FU release from P-P-FA-5FU and P-P-FA-Suc-5FU were studied in phosphate buffer saline (PBS, pH = 7.4 and pH = 5.02) as the release medium at pH = 7.4, pH = 5.02 and 37 °C. 3 mg of synthesized nanocarriers were suspended in 2 ml of PBS and replaced in a washed dialysis tubing (12,000 Da) and immersed in 30 ml of the release media (PBS). Then, the system was placed in an incubator shaker set at 40 rpm and 37 °C. At predetermined time intervals, 200 μl of the release medium was removed and replaced with the fresh medium. Aliquots of these formulations were collected at different time intervals up to 54 h, and the drug content was estimated by means of a Nanodrop UV-visible spectrophotometer at 266 nm using water as a control (Das et al. 2010).

2.4 Cell culture

The mouse breast cancer 4 T1, human breast adenocarcinoma MDA-MB-231 cell line and myoblast normal C2C12 cell lines were bought from the Pasteur Institute of Iran. The 4 T1 and C2C12 cells were maintained in RPMI and DMEM (Gibco, UK) respectively, supplemented with 10% fetal bovine serum (FBS), 2 mM glutamine, 100 μg/ml streptomycin, and 100 IU/ml penicillin.

2.5 Cellular uptake

Uptake studies of P-P-FA-^{99m}Tc were performed using PBS 1X and NaOH 0.1 M. For this assessment, C2C12 and 4 T1 cells were harvested and re-suspended at 5 × 10 (Ferlay et al. 2013) cells/300 μl in medium and cultured in 24 well plates. After 24 h, 500 nM (175 μCi), 250 nM (90 μCi), and 125 nM (50 μCi) of conjugate were added to each well and incubated at 37 °C. At various lengths of time (1, 3 and 24 h), the RPMI and DMEM media in the wells were removed and the medium activity, as a non-uptake drug conjugate, was read by means of a γ-counter. Afterward, the cultured cells in all the wells were washed with 250 μl of filtered PBS 1X, incubated for 15 min, 400 μl NaOH 0.1 M was used to separate the well-plate cells, and the cell activity was counted via the γ-counter as the uptake and receptor-conjugated carriers. The differences between the two activities were considered as an internalized P-P-FA-Suc-^{99m}Tc (Guo et al. 2011).

2.6 MTT assay

The growth inhibitory effects of PAMAM G4, P-P, P-P-FA, P-P-FA-5FU, P-P-FA-Suc-^{99m}Tc and P-P-FA-5FU-Suc-^{99m}Tc with 1000, 500, 250, 125, and 62.5 nM concentrations on 4 T1, MDA-MB-231 and C2C12 cells were assessed using the MTT assay. Every run was repeated nine times. Briefly, the cells were seeded in each well of 96-well microtiter plates and allowed to attach themselves overnight. Afterward, the cells were treated with different types of drugs that have already been mentioned. These drugs were added to the cultured cells at 24, 48, and 72 h. The process was repeated thrice. After that, the MTT solution (5 mg/ml in PBS) was added to each well and the cells were incubated for another four hours. Consequently, the suspension liquid was removed and the cells were re-suspended in DMSO. The optical density (OD) of these DMSO solutions was read at 570 nm. The difference

of the OD values between the treated and non-treated cells reflects the viability of well-cultured cells after treatment and, thus, stands for the metabolite toxicity.

2.7 Mouse model with breast tumor

Five- to six-week-old female BALB/c mice (average body weight 16.0 ± 1.5 g) were used for the *in-vivo* studies. The tumor was established by the subcutaneous injection of a 4 T1 tumor cell line on the right side of the post-neck region. The 4 T1 cell line, as a kind of mouse breast carcinoma that overexpresses folate receptors, was grown continuously as a monolayer at 37 °C and 5% CO2 in RPMI 1640 medium supplemented with penicillin (100 units/ml), streptomycin (100 μg/ml), and 10% heat-inactivated fetal bovine serum (FBS). The 4 T1 cells were prepared for the injection in the female BALB/c mice. 2 ml of 0.25% trypsin/1 mM EDTA solution was added to the plate, swirled to cover it, and incubated at room temperature for two minutes, followed by the addition of 5–6 ml serum-free medium to harvest trypsinized cells from the plate and transfer them to a conical tube. These cells were centrifuged for five minutes at 1000 rpm (25 °C). The supernatant was discarded and the pellet was re-suspended in a serum-free medium. The cells were diluted with serum-free medium to the desired concentration (1×10^6 cells/0.2 ml). These 4 T1 tumor cells in the serum-free medium suspension were inoculated in the subcutaneous space in the right post-neck side of the mice. Then, the mice were monitored daily for tumor onset by palpating the injection area with the index finger and thumb for the presence of the tumor. Twelve to 15 days after inoculation, the mice injected with 4 T1 cells developed palpable solid tumors. The mice tumor inhibition studies were performed when the tumor volume reached 619.2 ± 98.5 mm^3. Furthermore, the biodistribution efficiency of synthetic nano-complex was evaluated in tumor-bearing mice ($n = 12$) after 24 h of intravenous (IV) injection. As the radioactivity of nano-complex accumulated organs including tumor, liver, lung, kidney, and spleen was detected by means of γ-counter and outputs were asserted as percentages of the injected dose per gram (%ID/) organs.

2.8 Statistical analyses

Comparisons between the groups are expressed as the mean ± standard error of the mean. Statistical differences were evaluated using one-way ANOVA and Tukey's HSD with the considered significance at $p < 0.05$. All figures shown were obtained from three independent experiments. Any images shown are representative of the entire experiment.

3 Results and discussion

3.1 TGA analysis and drug loading efficiency

The contents of 5FU loading and FA in the synthetic nano-complex were estimated by means of TGA (heating-cooling process) with the observation of the partial fraction in the drug and the FA-encapsulated out coming peaks. From Fig. 1 A, which shows the TGA curves of freeze-dried samples, the stability and loading were estimated (Chang et al. 2012; Dong and Feng 2005; Baek et al. 2012). For the P-P sample, about 60.18% of the weight loss was observed at the 198–464 °C temperature range. The weight loss value of the P-P-

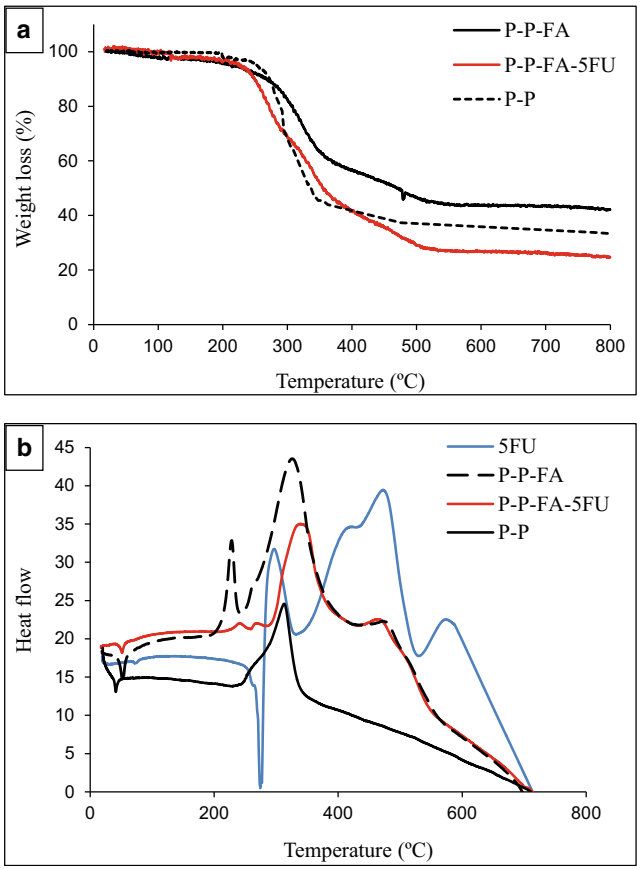

Fig. 1 TGA curves (A) and DSC termograms (B) of P-P, P-P-FA, P-P-FA-5FU, and pure 5FU. For the P-P sample, about 60.18% of the weight loss was observed at the 198–464 °C temperature range. The weight loss value of the P-P-FA sample was obtained in three phases (2% at 100 °C, 36.2% at 220–375 °C and 14.18% at 375–526 °C). With compare the P-P-FA and P-P-FA-5FU curves after finishing the weight loss, the estimated drug loading was about 16.97%. About 69.08% of the weight loss of P-P-FA-5FU nano-complex was significantly occurred at 188–510 °C. On the other hand, The DSC curve of pure 5FU showed an endothermic peak at 280 due to 5FU crystals melting and an exothermic peak at 335 °C, indicating its thermal decomposition. The elimination of this peak on the P-P-FA-5FU curve shown deformation (decrystallization) of 5FU after loading, confirming excellent drug-loading. Furthermore, a comparison of the P-P-FA with the FA curve demonstrated consistent conjugation of FA to P-P-FA, resulting from two endothermic peaks at 230–350 °C

FA sample was obtained in three phases. The first one was about 2% at 100 °C which was related to water evaporation. The second one happened at 220–375 °C, exhibiting about 36.2% of the weight loss, and the third one at the 375–526 °C range was related to 14.18% of the sample weight loss. About the P-P-FA-5FU curve, 2.7% of the weight loss around 100 °C was considered as water evaporation and about 69.08% of the weight loss occurred at 188–510 °C. Also, by considering the P-P-FA and P-P-FA-5FU curves after finishing the weight loss, the estimated drug loading was about 16.97%.

3.2 Drug-release profile

Figure 2 indicates the *in-vitro* release of the 5FU into the PBS solution from drug-loaded P-P-FA-5FU, P-P-FA-5FU-Suc-^{99m}Tc, and pure 5FU. A controlled release profile was demonstrated for both P-P-FA-5FU and P-P-FA-5FU-Suc-^{99m}Tc, and more than all for P-P-FA-5FU-Suc-^{99m}Tc. About 50% of the pure drug was released rapidly in the first 2.5 h, while these release values of P-P-FA-5FU and P-P-FA-5FU-Suc-^{99m}Tc were obtained at 7.5- and 11-h tube dialyzing at pH = 7.4. On the other hand, more than 50% of drug release of P-P-FA-5FU and P-P-FA-5FU-Suc-^{99m}Tc nano-complexes was obtained in first 5 h at pH = 5.02 that was faster than drug release at pH = 7.4. These controlled and sustained release behavior are more important to long-term drug release in human body serum and decrease the side effects of chemotherapeutic agents on normal cells (Chang et al. 2012; Baek et al. 2012). More than 90% of pure 5FU escaped within the first 8.5 h. The release profile of P-P-FA-5FU showed a rapid release of 5FU—about 80% within the first 16 h—but a shoulder slowly appeared in the release curve at 16 to 54 h with about 15% release at pH = 7.4. The initial fast release behavior of P-P-FA-5FU and P-P-FA-5FU-Suc-^{99m}Tc nano-complexes is owing to weakly adsorbed 5-FU molecules at the surface of the nano-complexes as shown in Fig. 2. The P-P-FA-5FU-Suc-^{99m}Tc compound generally indicated a slower release than the previous compound. Near 80% of the drug was released within the first 20 h, and after this time, the release profile showed control, up to 93.5% (total release). On the other hand, the pH-sensitive release behavior of 5-FU is favorable for burst drug release in the acidic environment of endosomes of cancer cells (Dong and Feng 2005). Furthermore, slow release behavior is suitable for long-time remain of drug in the plasma at physiological conditions (pH 7.4). Almost the same results were reported for the dendrimer-based release profile of Yulei Chang and Yongli Zheng et al. But, our release profile showed a higher total and controlled drug release compared with their works (Chang et al. 2012). Furthermore, our synthetic nano-complexes were demonstrated the slower release at the first 10 h in comparison to polymeric nano-complex that synthesized by Hu et al. (Hu et al. 2017) On the other hand, their nano-complex have been shown about 10% of total release at the end time, while it was about 85% for P-P-FA-5FU nano-complex in this research.

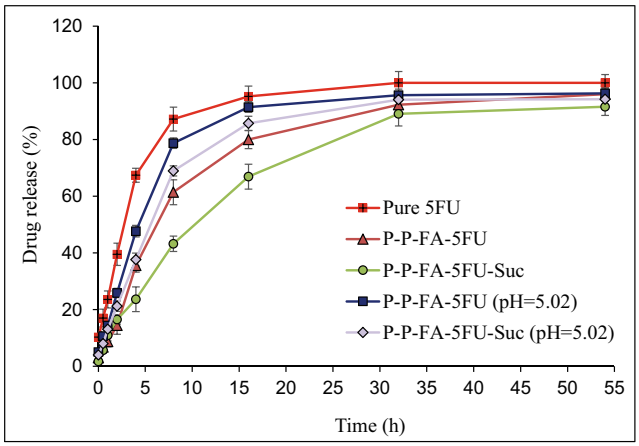

Fig. 2 *In vitro* profile of 5-FU release at pH = 7.4 and 5.02. Near 50% of the pure drug was released rapidly in the first 2.5 h and more than 90% of pure 5FU escaped within the first 8.5 h. While these release values of P-P-FA-5FU and P-P-FA-5FU-Suc were obtained at 7.5- and 11-h tube dialyzing. On the other hand, more than 50% of drug release of P-P-FA-5FU and P-P-FA-5FU-Suc-^{99m}Tc nano-complexes was obtained in first 5 h at pH = 5.02 that is faster than drug release at pH = 7.4. More than 90% of pure 5FU escaped within the first 8.5 h. The release profile of P-P-FA-5FU indicated a rapid release of 5FU—about 80% within the first 16 h—but a shoulder slowly appeared in the release curve at 16 to 54 h with about 15% release. However, P-P-FA-5FU-Suc nano-complex generally demonstrated a slower release than the previous compound. As, about 80% of the drug was released within the first 20 h, and after this time, the release profile showed control, up to 93.5% (total release)

3.3 Physical status of synthetic nanoparticles (DSC)

The physical states of the different synthetic samples were analyzed via the DSC device (Fig. 1 B) (Baek et al. 2012). We focused on the loading and conjugation of a drug and other legend results in the absence or shifting of endothermic peaks, indicating a change in the crystal lattice, melting, boiling, or sublimation points, which could provide both qualitative and quantitative information of the drug and conjugations present in the complexes (Horvath et al. 2008). The DSC curve of pure 5FU showed an endothermic peak at 280 °C due to 5FU crystals melting and an exothermic peak at 335 °C, indicating its thermal decomposition. The elimination of this peak on the P-P-FA-5FU curve revealed deformation (decrystallization) of 5FU after loading, confirming excellent drug-loading (Navath et al. 2011). A comparison of the P-P-FA with the FA curve revealed consistent conjugation of FA to P-P-FA, resulting from two endothermic peaks at 230–350 °C. The large second peak of the P-P-FA, in comparison with pure FA, is due to the FA and PEG melting point overlapping and their deformation. The P-P complex indicated an endothermic peak at 250 °C, which is related to the melting point of PEG.

About the stability of nanocomplexes, the DSC curves' expected results exhibited an increase in the stability of the final nanocomplexes compared to pure compounds, presumably due to the incorporated complexity and the generation of a homogenous structure.

3.4 PBS and serum stability

The radiochemical stability for both P-P-FA-Suc-^{99m}Tc and P-P-FA-5FU-Suc-^{99m}Tc was evaluated by ITLC at the time-points of 1, 2, 4, and 24 h. As Fig. 3 A and B shows, both samples exhibited excellent radiochemical stability even for extended periods. After the incubation of P-P-FA-Suc-^{99m}Tc and P-P-FA-5FU-Suc-^{99m}Tc (200 μCi) in PBS and serum at 37 °C for up to 24 h, more than 76% of the total radioactivity was conserved. Generally, stability was about 85.28 ± 1.99% and 85.32 ± 1.15% in PBS and 86.67 ± 2.11% and 83.75 ± 0.88% in the serum samples after an hour for P-P-FA-Suc-^{99m}Tc and P-P-FA-5FU-Suc-^{99m}Tc nano-complexes respectively. Also, we obtained 77.2 ± 0.76% and 77.98 ± 0.74% in PBS and 76.27 ± 1.02% and 78.35 ± 1.47% in the serum samples after 24 h for the P-P-FA-Suc-^{99m}Tc and the P-P-FA-5FU-Suc-^{99m}Tc nano-complex, respectively. The stability of the P-P-FA-Suc-^{99m}Tc nano-complex in the first one and two hours in serum was more than PBS; however, for the P-P-FA-5FU-Suc-^{99m}Tc complex, the serum stability was less, presumably due to the 5FU physical bond that contacts with stable radio-labeling. These values of stability are consistent with the same stability assay in antibody-labeled stability, which indicated that the nanoparticles can be considered as

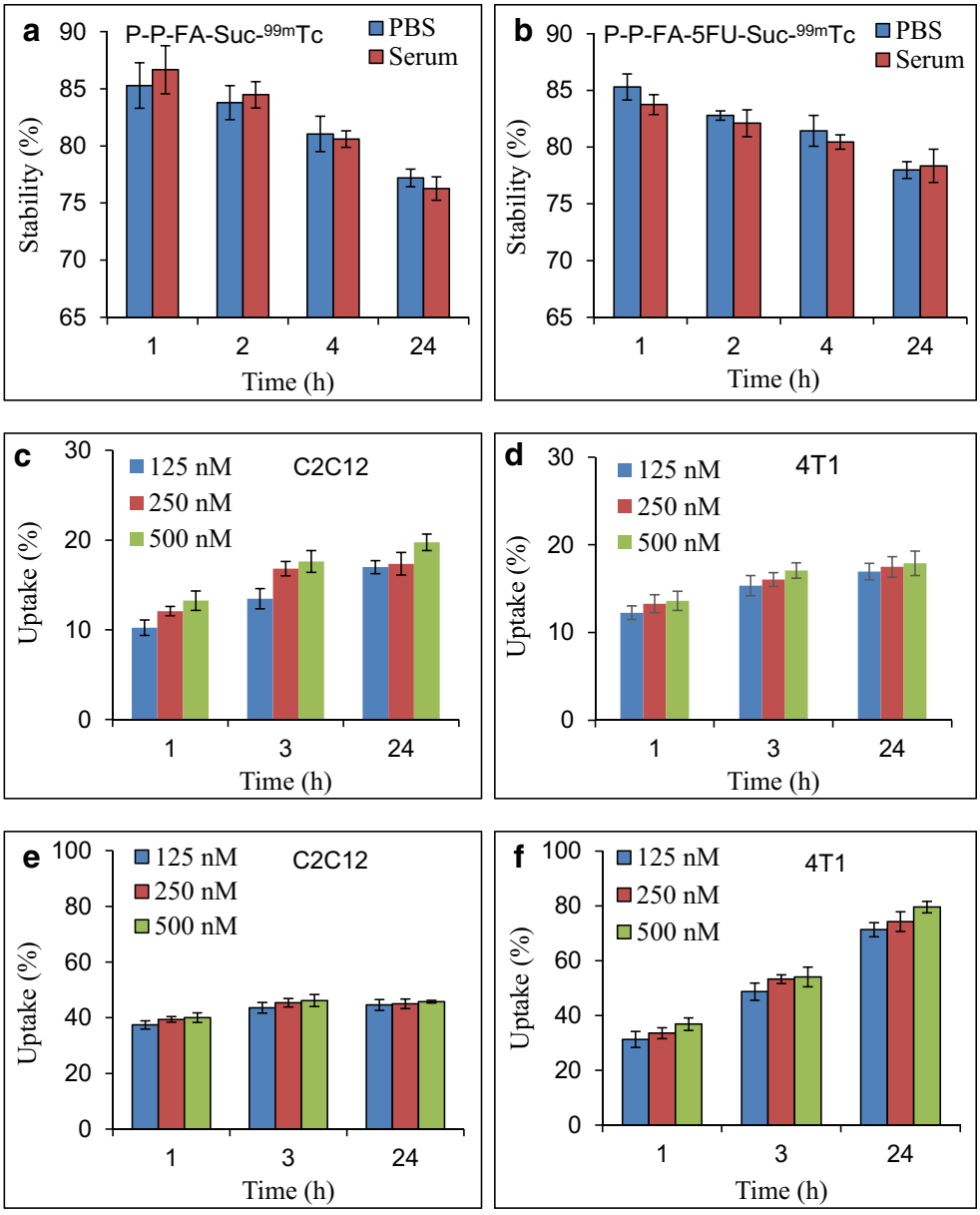

Fig. 3 Serum stability and cellular uptake of nano-complex. PBS and serum stabilities of ^{99m}Tc radiolabeled drug samples (A and B). It is clear that after the incubation of P-P-FA-Suc-^{99m}Tc and P-P-FA-5FU-Suc-^{99m}Tc (200 μCi) nano-complexes in PBS and serum at 37 °C for up to 24 h, more than 76% of the total radioactivity was conserved. On the other hand, the stability of the P-P-FA-^{99m}Tc nano-complex in the first one and two hours in serum was more than PBS; while for the P-P-FA-5FU-^{99m}Tc complex, the serum stability was less, presumably due to the 5FU physical bond that contacts with stable radio-labeling. C2C12 and 4 T1 cell uptake percentage in 125, 250 and 500 nM concentrations after 1, 3 and 24-h interval times (E and F are relate to P-P-FA-^{99m}Tc, and C and D are relate to PAMAM-^{99m}Tc). A comparison of the end uptake time indicated the main difference between the normal and cancer cell uptakes. As, a 16.12% uptake increase was calculated for 125 nM after 24 h, while for 500 nM, it was 12.52%. However, these values were calculated as 40.09% (125 nM) and 42.7% (500 nM) for 4 T1 cell lines. These data indicate that the nano-complex can target the FR specifically and be highly internalized in the 4 T1 cells rather than C2C12

good candidates for radio-labeling (Alirezapour et al. 2016). Generally, a decrease in the stability after 24 h could be due to protein interactions, such as albumin in serum (Song et al. 2017; Alirezapour et al. 2016).

3.5 Cellular uptake

To determine the positive effect of FA-targeted nanocarriers in cellular internalization, we investigated the ability of these nono-complexes to be endosytozed by cells (Fig. 3 C and D). Our results depicted a robust uptake of the P-P-FA-Suc-^{99m}Tc by the 4 T1 cancer cell lines (about 79.58 ± 2.12% in 500 nM concentrations after 24 h) and C2C12 normal (about 45.74 ± 0.48% in 500 nM concentrations after 24 h) as a control cell line. However, the complex uptake of C2C12 was higher than the 4 T1 cell line in the first hour. A comparison of the end uptake time revealed the main difference between the normal and cancer cell uptakes. For example, the C2C12 exhibited more uptake at 125 nM compared with other concentrations after 24 h. As, a 16.12% uptake increase was calculated for 125 nM after 24 h, while for 500 nM, it was 12.52%. However, these values were calculated as 40.09% (125 nM) and 42.7% (500 nM) for 4 T1 cell lines. Both 4 T1 and C2C12 cell lines express FRs, though it is higher in 4 T1 cell lines (Zheng et al. 2016; Narmani et al. 2018b). On the other hand, the uptake evaluation of PAMAM-Suc-^{99m}Tc nano-complex was indicated very low (less than 3-folds) cellular internalization in comparison to P-P-FA-Suc-^{99m}Tc ones. This result was shown that FA has the main role in internalization pathway. These *in vitro* cellular uptake results were consistent with a research by Zheng et al. As the blockage of cell surface receptor lead to decrease the rate of internalization efficiency (Zheng et al. 2016). The same results can also obtain without the presence of FA as a targeting factor. These data exhibit that the complex can target the FR specifically and be highly internalized in the 4 T1 cells rather than C2C12 (Guo et al. 2011). As we have noted previously, it is well known that FRs are overexpressed in various human cancer cells.

3.6 Cell-viability assay

The MTT assay was performed to evaluate the cytotoxicity of P-P-FA-5FU-Suc-^{99m}Tc conjugates against C2C12, MDA-MB-231 and 4 T1 cells using the cytotoxicity of 5FU-loaded ligands and ^{99m}Tc conjugates as therapeutic agents. Previous research has revealed that the electrostatic interactions between positively charged complexes and negatively charged cell membranes result in cell morphological changes, membrane damage, and finally, cell apoptosis. Our research is an evidence of the effects of all six types of conjugates on the viability of C2C12, MDA-MB-231 and 4 T1 cells measured by the MTT assay. Figure 4 shows the cell viability results. We believe that the low cytotoxicity is mainly associated with the ligands and PEG chains linked to the dendrimers, which can effectively reduce the cytotoxic effects of the conjugates. For the 4 T1 cell lines, pure PAMAM G4 toxicity was changed at 62.5 and 1000 nM concentrations with 45–60% viability, respectively. After PEGylation, cell viability increased up to about 27% (81.53%, 85% and 83.57% at 1000 nM for MDA-MB-231, 4 T1 and C2C12, respectively). However, at a 62.5 nM concentration, we observed no rising cell viability (Chang et al. 2012). Obviously, high concentrations of P-P-FA nano-complex increase the cytotoxic effect of the conjugate because an increase in the cellular uptake via targeting ligands results in increasing cytotoxic effects of PAMAMG4. The FA results were different compared with the two drug samples. In fact, at 250 nM concentration of P-P-FA, high cell viability was obtained against our expectation. At 1000 and 62.5 nM (about 72%, 59% and 63% viability for MDA-MB-231, 4 T1 and C2C12, respectively), there was no indication of any cell viability values, while FA and PEG were considered as biomaterials. These are due to low concentrations of PEG and FA at 62.5 nM and high concentrations of FA at 1000 nM, which leads to an increase in the PAMAM internalization and its toxic effect, especially about the 4 T1 cell line. These results were not consistent with Yulei Chang et al.'s work (Chang et al. 2012). The P-P-FA-5FU conjugate has an inhibitory effect on the cell lines in gradian-dependent concentrations, specifically in high concentrations related to 5FU as a chemotherapeutic agent (about 24% and 14% viability for 4 T1 cell line at 62.5 and 1000 nM concentrations). Furthermore, the cell viability was by 19% and 16% at 62.2 and 1000 nM for MDA-MB-231 breast cancer cell line. The 4 T1 and MDA-MB-231cell lines showed more sensitiveness than C2C12 in viability at all concentrations. The cytotoxic evaluation of nano-complexes was compared with a study by Hu et al. which has been evaluated the cytotoxicity of Doxorubicin (DOX) loaded polymer on Hela cell line (Dong and Feng 2005). A comparison of the 4 T1 and MDA-MB-231 cancer cell lines with Hela cell line regarding the effects of various types of nano-complex demonstrated that P-P-FA-5FU and P-P-FA-5FU-Suc-^{99m}Tc have more cytotoxic effects on 4 T1 and MDA-MB-231 cell lines in comparison with Hela cell line at the low concentrations of nano-complex (Dong and Feng 2005).

On the other hand, the P-P-FA-Suc-^{99m}Tc does not have any notable toxic effect in relation to the previous conjugate. However, ^{99m}Tc has been considered as a radioactive drug, and due to the low half-life of ^{99m}Tc (6 h), the viability assay was also made within three hours. After three hours, the P-P-FA-Suc-^{99m}Tc and P-P-FA-5FU-Suc-^{99m}Tc incubation cell viabilities obtained were about 96% and 80% at 62.5 nM and1000 nM, respectively (for C2C12, it was 95% and 86% for P-P-FA-Suc-^{99m}Tc and 92% and 81% for P-P-FA-5FU-Suc-^{99m}Tc). Moreover, the cell viability was exhibited by

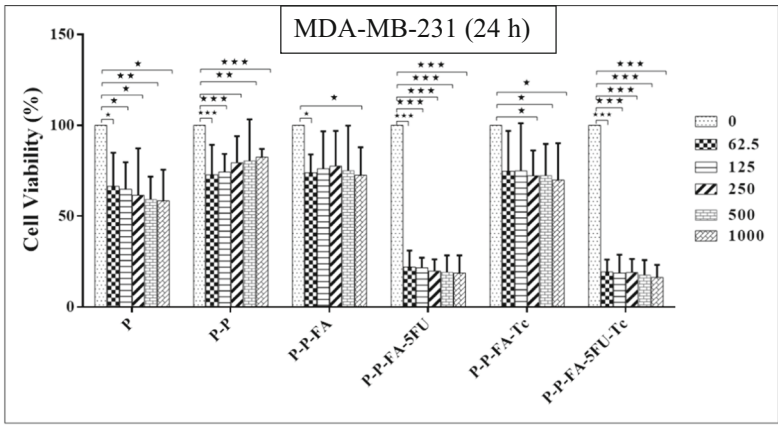

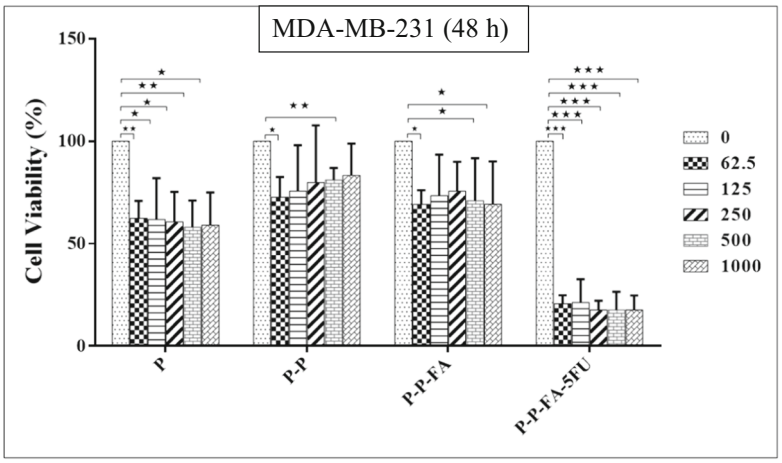

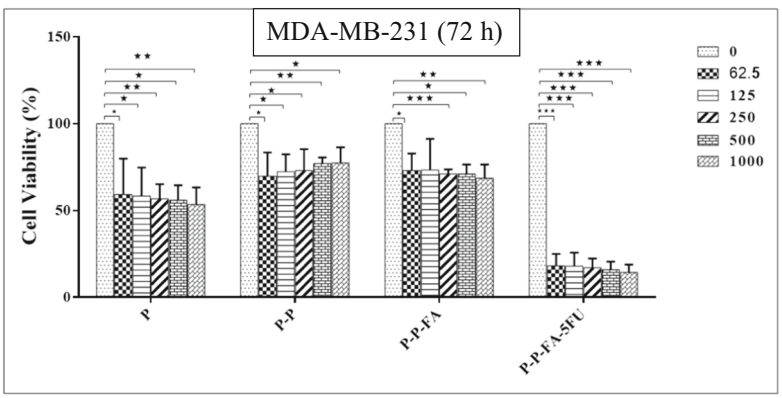

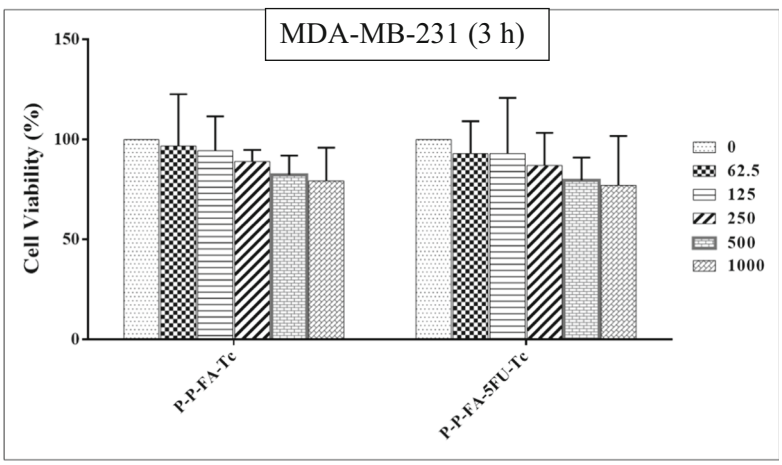

Fig. 4 The cytotoxic effect of pure P, P-P, P-P-FA, P-P-FA-5FU, P-P-FA-Suc-^{99m}Tc and P-P-FA-5FU-Suc-^{99m}Tc incubated with MDA-MB-231, 4 T1 and C2C12 cell lines. As indicated, the highest cytotoxicity effects are related to P-P-FA-5FU, P-P-FA-5FU-Suc-^{99m}Tc and PAMAM G4 in three cell lines. Negative concentration dependent behavior in cell growth inhibition show for P-P-FA-5FU, P-P-FA-5FU-Suc-^{99m}Tc and PAMAM G4, while it is positive in surface modified (P-P) and functionalized (P-P-FA) nano-complexes. For the 4 T1 cell lines, pure PAMAM G4 toxicity was changed at 62.5 and 1000 nM concentrations with 45–60% viability, respectively. After PEGylation, cell viability increased by 81.53%, 85% and 83.57% at 1000 nM for MDA-MB-231, 4 T1 and C2C12, respectively. The P-P-FA-5FU conjugate has an inhibitory effect on cell viability by 24% and 14% for 4 T1 cell line at 62.5 and 1000 nM concentrations. While it was about 19% and 16% at 62.2 and 1000 nM for MDA-MB-231 breast cancer cell line

Fig. 4 (continued)

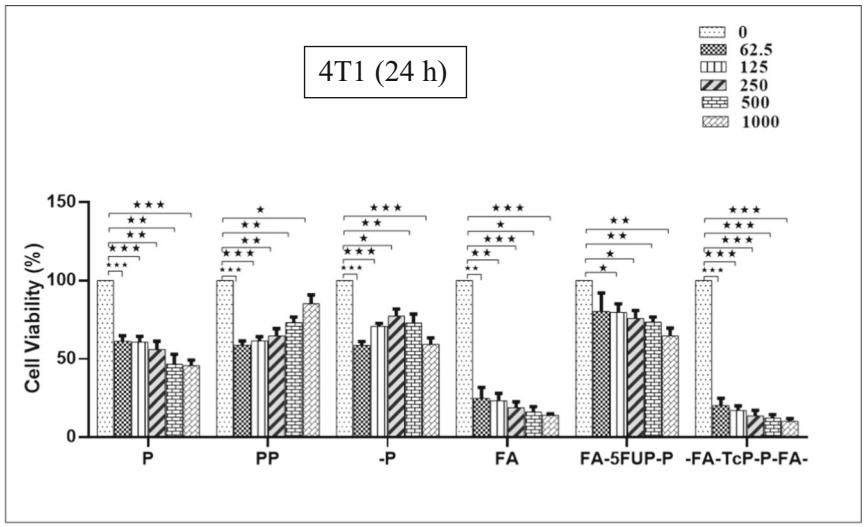

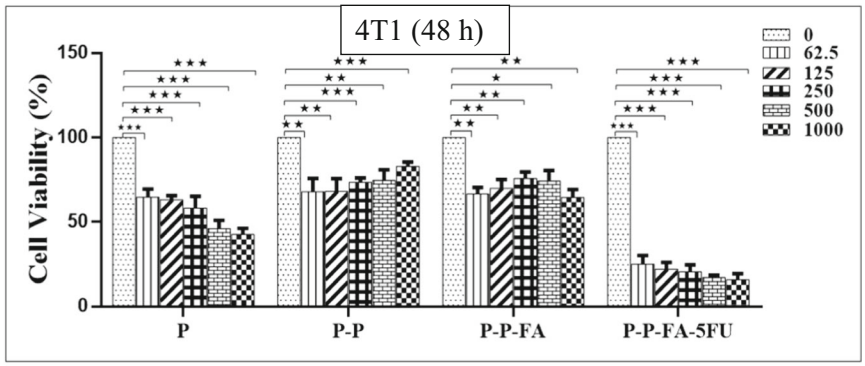

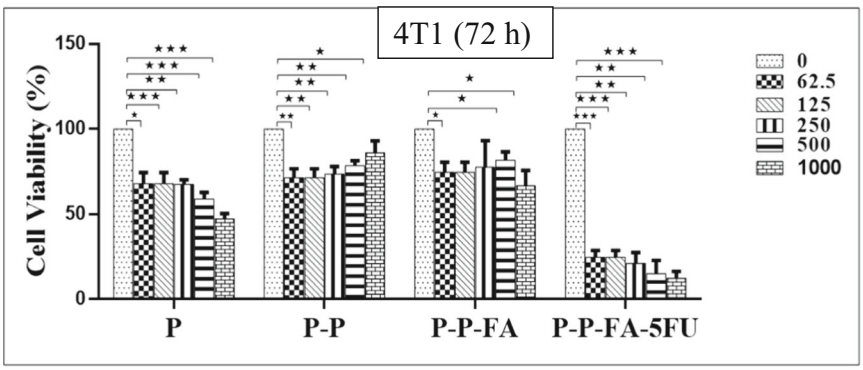

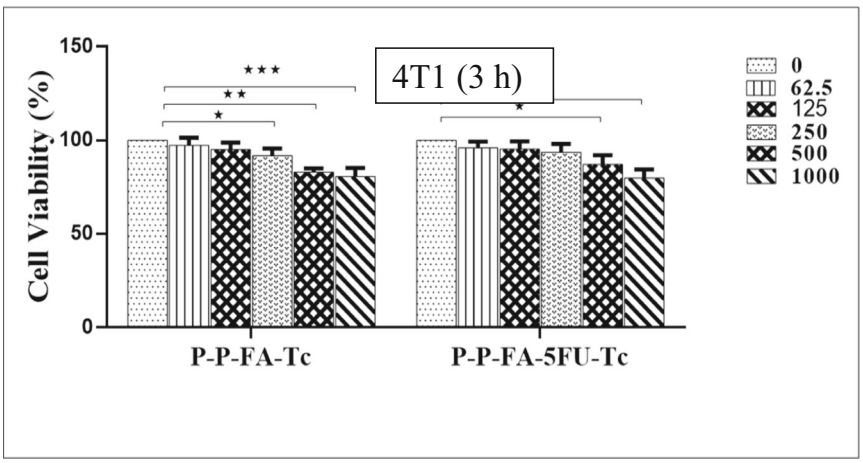

Fig. 4 (continued)

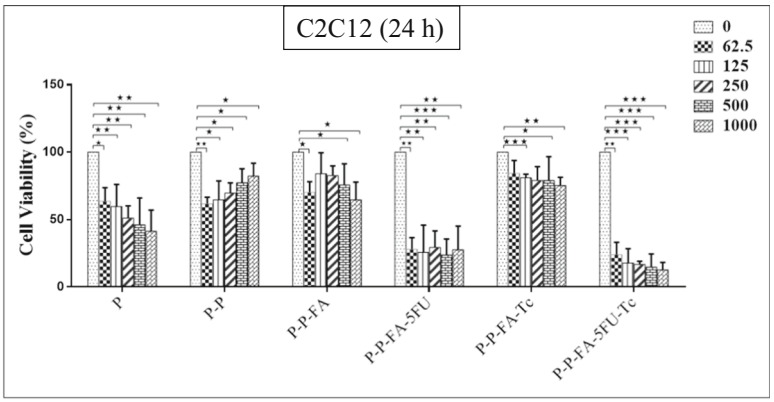

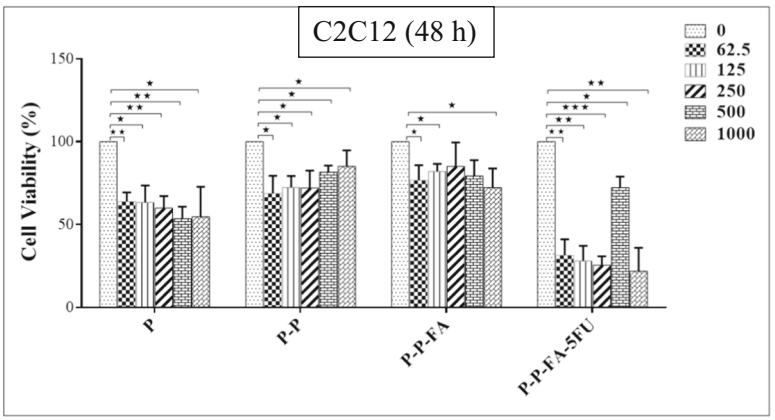

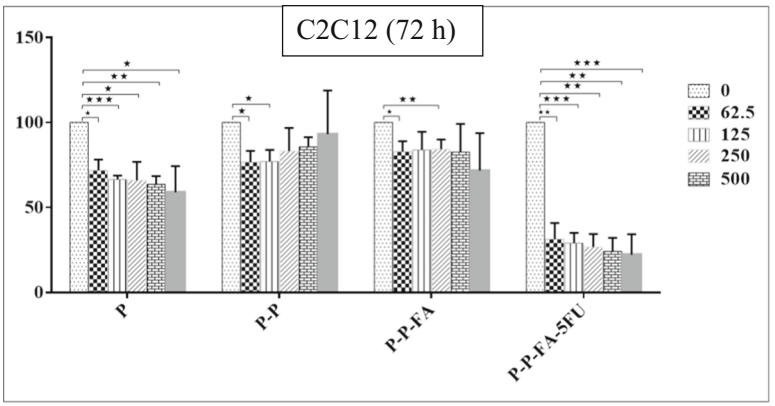

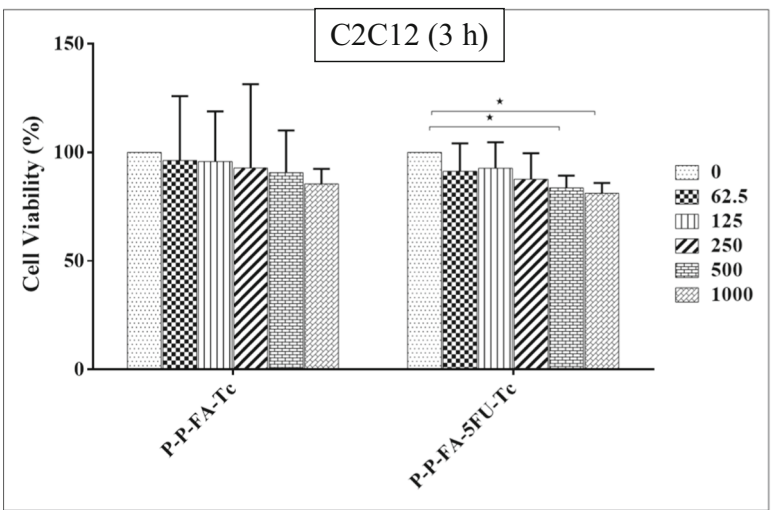

79% and 77% after treatment with P-P-FA-Suc-^{99m}Tc and P-P-FA-5FU-Suc-^{99m}Tc at 1000 nM for MDA-MB-231 cell line. Active drugs' cell-death activity between C2C12 and 4 T1 cell lines was different, as the 4 T1 cell line indicated sensitivity rather than the C2C12 cell line at 500 nM and 1000 nM. Our late synthesis showed a higher cytotoxic effect in relation to all of our conjugates, which was due to the combined effect of 5FU and ^{99m}Tc as the chemotherapeutic agents. Also, cell viability was assessed at 48 and 72 h. Generally, P-P-FA-5FU-Suc-^{99m}Tc due to active γ-ray emission damaged the DNA structure, replication, and cell division, which led to the improvement of the 5FU drug as a main therapeutic agent. Also, we concluded that all drug types could inhibit the MDA-MB-231 and 4 T1 cell line compared to the C2C12 cell line, which may be due to the high replication and uptake rate in the 4 T1 cell line.

Treatment with six types of drug complexes indicated inhibited cell viability compared with the control (non-injected) group after treatment initiation and had statistically significant differences ($p < 0.05$) in cell viability. The MDA-MB-231 and 4 T1 statistical Fisher's exact test (F-test) was calculated at 5.00 ($p < 0.01$) by the drugs with a lower viability mean (Dong and Feng 2005) for the P-P-FA-5FU-Suc-^{99m}Tc at 24 h. For C2C12, the F-test value was 6.00 ($p < 0.05$) by the drugs with a viability mean of 30 for P-P-FA-5FU-Suc-^{99m}Tc, as a more inhibiting drug.

3.7 Treatment of mouse model with breast tumor and *in vivo* toxicity

The treatment of the mouse model with a breast tumor was examined via the intravenous injection of P-P-FA-5FU and P-P-FA-5FU-Suc-^{99m}Tc as drug samples and PBS as a control. The *in vivo* behavior of nanoparticles often differs significantly from the predicted behavior derived from *in-vitro* cell-culture studies (Satsangi et al. 2015; Sayes et al. 2007). Firstly, 4 T1 cells were injected into the BALB/c mice and the tumor cells' growth was monitored daily. According to the reports, the 4 T1 cells were highly metastatic breast cancer cells, and the MMP secretion and the activities were very high (Song et al. 2017). Twelve to 15 days after the 4 T1 cells' injection, the tumor masses were observed in the mice ($n = 15$). Secondly, the tumor-bearing mice were randomly divided into three groups ($n = 5$ in every group), and each group was treated with the P-P-FA-5FU, P-P-FA-5FU-Suc-^{99m}Tc, and PBS, separately. The mice were treated with drug samples at two interval times (6 days). Then, the inhibition of the tumor size was monitored every day up to 21 days. Both drug-loaded samples showed an inhibitory effect on tumor growth and decreased the tumor volume size 21 days after the monitoring period (Fig. 5). The tumor size was calculated via the following formula: (Vredenburg et al. 2001)

$$\text{Tumor size} = 0.4\left(\text{L.W}^2\right)$$

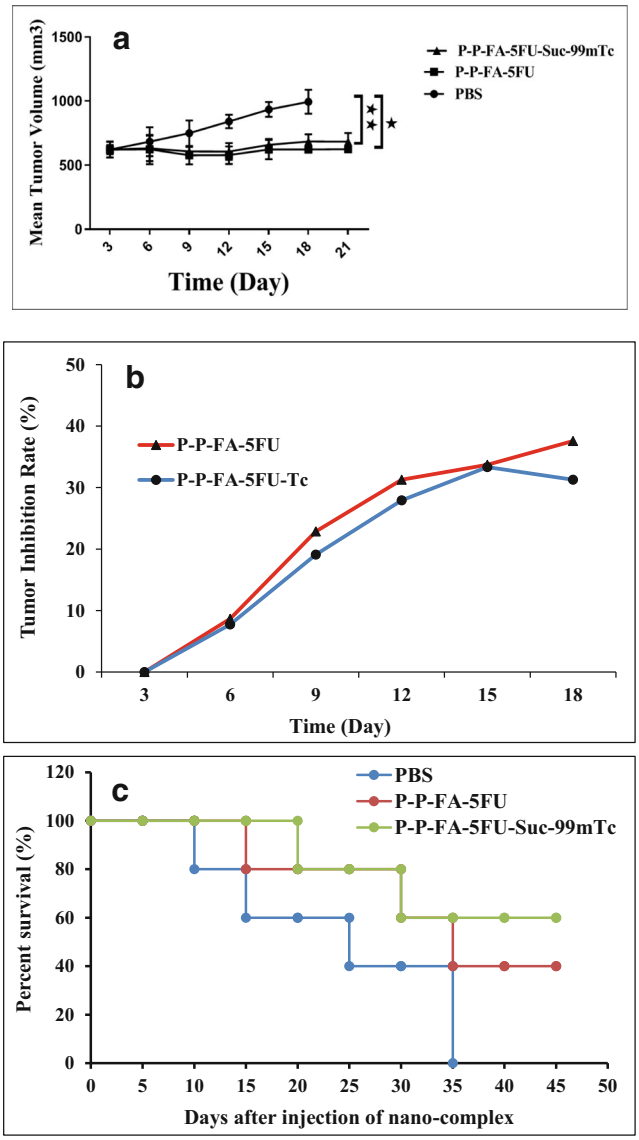

Fig. 5 Mean tumor volume (A), tumor inhibition rate (B), and survival curve (C) of tumor bearing BALB/C mice after treatment with PBS (as control), P-P-FA-5FU and P-P-FA-5FU-Suc-^{99m}Tc synthetic drugs. Both P-P-FA-5FU (23.23%) and P-P-FA-5FU-^{99m}Tc (25.74%) nano-complexes exhibited excellent tumor-inhibition activity and reduced growth in the tumor volume. As the tumor volume diminished from 619.2 ± 98.5 to 576.6 ± 60.4 mm^3 (6.87% reduced tumor volume) for P-P-FA-5FU at six to 12 days. However, for the P-P-FA-5FU-Suc-^{99m}Tc complex, there was little difference, as the tumor volume decreased from 619.2 ± 28 to 604.8 ± 24.2 mm^3 on Day 12 (2.32% reduced volume). Survival curves P-P-FA-5FU and P-P-FA-5FU-Suc-^{99m}Tc nano-complexes demonstrate that only 20% of mice are dead after 25 days of IV injection while it is about 60% for mice treated with PBS. Furthermore, mice treated with nano-complexes are alive after 45 days of injection that is 10 days more than PBS-treated mice

In which, L and W are abbreviations of the tumor's length and width respectively. Also, the tumor inhibition rate (TIR) was calculated as follows:

$$\mathrm{TIR}\ (\%) = V_1 - V_2 / V_1 \times 100$$

In which V_1 is the average volume of the tumors in the PBS group and V_2 is the average volume of the tumors in the treated groups. The result showed that the P-P-FA-5FU and P-P-FA-5FU-Suc-^{99m}Tc inhibited the growth of the breast tumors (Fig. 5). Hence, both P-P-FA-5FU and P-P-FA-5FU-Suc-^{99m}Tc showed excellent tumor-inhibition activity and reduced growth in the tumor volume (23.23% and 25.74% for P-P-FA-5FU and P-P-FA-5FU-Suc-^{99m}Tc respectively). However, P-P-FA-5FU-Suc-^{99m}Tc had the better tumor-inhibition effect of the two. Partially, the tumor volume decreased from 619.2 ± 98.5 to 576.6 ± 60.4 mm^3 (6.87% reduced tumor volume) for P-P-FA-5FU at six to 12 days (Fig. 5A). However, the tumor volume increased at Day 12 to 18 and reached 622.7 ± 63 on Day 21. For the P-P-FA-5FU-Suc-^{99m}Tc complex, there was little difference, as the tumor volume reduced from 619.2 ± 28 to 604.8 ± 24.2 mm^3 on Day 12 (2.32% reduced volume). But, the tumor volume increased up to 681.8 ± 59.3 mm^3 (10.1% volume increase) on Days 18 and 21. Both the nano-complexes showed a reduced tumor volume for the first time within Days 6 to 9. Moreover, survival curves P-P-FA-5FU and P-P-FA-5FU-Suc-^{99m}Tc nano-complexes demonstrate that only 20% of mice are dead after 25 days of IV injection while it is about 60% for mice treated with PBS (Fig. 5C). Furthermore, mice treated with synthetic nano-complexes are alive after 45 days of injection that is 10 days more than PBS-treated mice. Survival curve of P-P-FA-5FU-Suc-^{99m}Tc demonstrated 100% and 60% viability after 15 and 45 days of post-treatment which is considerably high potent and promising nano-complex for using as a therapeutic agent in cancer therapy.

besides, the percentage of injected dose per gram (%ID/g) of tumor, liver, lung, kidney, and spleen was also measured after 24 h of nano-complex intravenous administration. So that the organ accumulation evaluation profiles were shown that the radioactivity in the liver, lung, kidney, and spleen was $13.62 \pm 1.29\%$, $1.54 \pm 0.07\%$, $4.45 \pm 0.43\%$ and $3.28 \pm 0.28\%$ after 24 h of IV administration of radiolabeled nano-complex (P-P-FA-Suc-^{99m}Tc) in tumor-bearing mice, respectively. While the percentage of injected dose per gram of tumor tissue was $13.76 \pm 1.39\%$ at the same time.

Treatment with both drug complexes began to show a reduced growth in the tumor volume compared with the control group (PBS injections) three days after the initiation of treatment and had statistically significant differences ($p < 0.05$) in tumor volume by Days 3 to 21. Partially, the statistical F-test for the P-P-FA-5FU's and P-P-FA-5FU-Suc-^{99m}Tc's reduced tumor-growth volumes were calculated at 5.00 and 5.09 with a significance of 0.03 by time, respectively. Also, the F-test was calculated at 14 with a significance level of 0.05 by experiments for both nano-complexes.

4 Conclusions

In summary, the P-P-FA-5FU-Suc-^{99m}Tc and P-P-FA-Suc-^{99m}Tc nano-complexes were evaluated in drug loading efficiency, drug release behavior, stability, internalization, cancer cell inhibition ability, and tumor inhibition potency. The obtained drug loading was about 16% by means of TGA, and > 95% radio-labeling was calculated via γ-counter by the use of ITLC for the final nano-complex. The PBS and FBS stability analyses showed very good stability of the radio-labeled nanocarrier. The cellular uptake data revealed the effective efficiency of FA-targeted nanoparticles into the breast cancer cell internalization compared with the non-targeted nanocarrier and normal cells. Furthermore, the MTT assay of cell viability was implemented for P-P-FA-5FU-Suc-^{99m}Tc and its derivate, and we found that the PEGylation of nanoparticles increased the cell viability up to 50% and the FA molecules in the nanocarrier increased the cellular internalization. Also, cell viability assay of P-P-FA-5FU-Suc-^{99m}Tc and P-P-FA-Suc-^{99m}Tc nano-complexes indicated that ^{99m}Tc can be as anticancer agent in high dose. On the other hand, the breast tumor-bearing BALB/C mice showed an excellent tumor-inhibition rate and a decrease in size.

Acknowledgments This paper has been extracted from MSc thesis. The authors would like to acknowledge all the supports of University of Tehran. Tehran, Iran (Grant no. 28701/06/09).

Compliance with ethical standards

Conflict of interest The authors declare that they have no conflict of interest.

References

P. Agrawal, U. Gupta, N.K. Jain, Glycoconjugated peptide dendrimers based nanoparticulate system for thedelivery of chloroquine phosphate. Biomaterials **28**, 3349 (2007)

B. Alirezapour, M.J. Rasaee, A.R. Jalilian, S. Rajabifar, J. Mohammadnejad, M. Paknejad, E. Maadi, S. Moradkhani, Development of [64Cu]-DOTA-PR81 radioimmunoconjugate for MUC-1 positive PET imaging. J. Nucl. Med. Biol. **43**, 73 (2016)

A. Amini, M. Kamali, B. Amini, A. Najafi, A. Narmani, L. Hasani, J. Rashidiani, et al., Bio-barcode technology for detection of Staphylococcus aureus protein a based on gold and iron nanoparticles. Int. J. Biol. Macromol. **124**, 1256 (2019)

M. Baek, J.H. Choy, S.J. Choi, Montmorillonite intercalated with glutathione for antioxidant delivery: Synthesis, characterization, and bioavailability evaluation. Int. J. Pharm. **425**, 29 (2012)

E. Blanco, H. Shen, M. Ferrari, Principles of nanoparticle design for overcoming biological barriers to drug delivery. Nat. Biotechnol. **33**, 941 (2015)

Y. Chang, N. Liu, L. Chen, X. Meng, Y. Liu, Y. Li, J. Wang, Synthesis and characterization of DOX-conjugated dendrimer-modified magnetic iron oxide conjugates for magnetic resonance imaging, targeting, and drug delivery. J. Mater. Chem. **22**, 9594 (2012)

X. Cui, L. Dong, S. Zhong, C. Shi, Y. Sun, P. Chen, Sonochemical fabrication of folic acid functionalized multistimuli-responsive magnetic graphene oxide-based nanocapsules for targeted drug delivery. Chem. Eng. J. **326**, 839 (2017)

R.K. Das, N. Kasoju, U. Bora, Encapsulation of curcumin in alginate-chitosan-pluronic composite nanoparticles for delivery to cancer cells. Nanomedicine: NBM **6**, 153 (2010)

Y. Dong, S.S. Feng, Poly(D,L-lactide-co-glycolide)/montmorillonite nanoparticles for oral delivery of anticancer drugs. Biomaterials **26**, 6068 (2005)

J.C. Evans, M. Malhotra, J. Guo, J.P. O'Shea, K. Hanrahan, A. O'Neill, Folate targeted amphiphilic cyclodextrin-siRNA nanoparticles for prostate cancer therapy exhibit PSMA mediated uptake, therapeutic gene silencing *in vitro* and prolonged circulation *in vivo*. Nanomedicine **12**, 2341 (2016)

J. Ferlay, I. Soerjomataram, M. Ervik, R. Dikshit, S. Eser, C. Mathers, GLOBOCAN 2012 v1.0, Cancer Incidence and Mortality Worldwide: IARC Cancer Base No. 11 [Internet]. Lyon, France: International Agency for Research on Cancer; 2013**.** Available from: http://globocan.iarc.fr

C. Gómez-Canela, G. Bolivar-Subirats, R. Tauler, S. Lacorte, Powerful combination of analytical and chemometric methods for the photodegradation of 5-fluorouracil. J. Pharm. Biomed. Anal. **137**, 33 (2017)

H. Guo, F. Xie, M. Zhu, Y. Li, Z. Yang, X. Wang, J. Lu, The synthesis of pteroyllys conjugates and its application as technetium-^{99m} labeled radiotracer for folate receptor-positive tumor targeting. Bioorg. Med. Chem. Lett. **21**, 2025 (2011)

G. Horvath, T. Premkumar, A. Boztas, E. Lee, S. Jon, K.E. Geckeler, Supramolecular nanoencapsulation as a tool: Solubilization of the anticancer drug trans-dichloro (dipyridine) platinum (ii) by complexation with bcyclodextrin. Mol. Pharm. **5**, 358 (2008)

R. Hu, H. Zheng, J. Cao, Z. Davoudi, Q. Wang, Self-assembled hyaluronic acid nanoparticles for pH-sensitive release of doxorubicin: Synthesis and *in vitro* characterization. J. Biomed. Nanotechnol. **13**, 1058 (2017)

N. Leelakanok, S. Geary, A. Salem, Fabrication and use of PLGA-based formulations designed for modified release of 5-fluorouracil. J. Pharm. Sci. **107**, 513 (2017)

S. Liu, D.S. Edwards, M.C. Ziegler, A.R. Harris, S.J. Hemingway, J.A. Barrett, ^{99m}Tc-labeling of a hydrazinonicotinamide-conjugated vitronectin receptor antagonist useful for imaging tumors. Bioconjug. Chem. **12**, 624 (2001)

D. Luong, P. Kesharwani, R. Deshmukh, M.C.I. Mohd Amin, U. Gupta, K. Greish, et al., PEGylated PAMAM dendrimers: Enhancing efficacy and mitigating toxicity for effective anticancer drug and gene delivery. Acta Biomater. **43**, 14 (2016)

S. Mombini, J. Mohammadnejad, B. Bakhshandeh, A. Narmani, J. Nourmohammadi, S. Vahdat, S. Zirak, Chitosan-PVA-CNT nanofibers as electrically conductive scaffolds for cardiovascular tissue engineering. Int. J. Biol. Macromol. **140**, 278 (2019)

A. Narmani, M. Kamali, B. Amini, H. Kooshki, A. Amini, L. Hassani, Highly sensitive and accurate detection of Vibrio cholera O1 OmpW gene by fluorescence DNA biosensor based on gold and magnetic nanoparticles. Process Biochem. **65**, 46 (2018a)

A. Narmani, B. Farhood, H. Haghi-aminjan, T. Mortezazadeh, A. Aliasgharzadeh, M. Mohseni, et al., Gadolinium nanoparticles as diagnostic and therapeutic agents: Their delivery systems in magnetic resonance imaging and neutron capture therapy. J. Drug Deliv. Sci. Technol. **44**, 457 (2018b)

A. Narmani, M. Kamali, Y. Panahi, B. Amini, A. Salimi, Targeting delivery of oxaliplatin with smart PEG-modified PAMAM G4 to colorectal cell line: *In vitro* studies. Process Biochem. **69**, 178 (2018c)

A. Narmani, J. Mohammadnejad, K. Yavari, Synthesis and evaluation of polyethylene glycol- and folic acid-conjugated polyamidoamine G4 dendrimer as nanocarrier. J. Drug Deliv. Sci. Technol. **50**, 278 (2019a)

A. Narmani, M. Rezvani, B. Farhood, P. Darkhor, J. Mohammadnejad, B. Amini, S. Refahi, et al., Folic acid functionalized nanoparticles as pharmaceutical carriers in drug delivery systems. Drug Dev. Res. **68**, 256 (2019b)

R.S. Navath, A.R. Menjoge, H. Dai, R. Romero, S. Kannan, R.M. Kannan, Injectable PAMAM dendrimer-PEG hydrogels for the treatment of genital infections: Formulation, *in-vitro* and *in-vivo* evaluation. Mol. Pharm. **8**, 1209 (2011)

M. Rezvani, J. Mohammadnejad, A. Narmani, K. Bidaki, Synthesis and *in vitro* study of modified chitosan polycaprolactam nanocomplex as delivery system. Int. J. Biol. Macromol. **113**, 1287 (2018)

A. Satsangi, S.S. Roy, R.K. Satsangi, A.W. Tolcher, R.K. Vadlamudi, B. Goins, J.L. Ong, Synthesis of a novel, sequentially active-targeted drug delivery nanoplatform for breast cancer therapy. Biomaterials **59**, 88 (2015)

C.M. Sayes, K.L. Reed, D.B. Warheit, Assessing toxicity of fine and nanoparticles: Comparing *in vitro* measurements to *in vivo* pulmonary toxicity profiles. Toxicol. Sci. **97**, 163 (2007)

E.I. Sega, P.S. Low, Tumor detection using folate receptor-targeted imaging agents. Cancer Metastasis Rev. **27**, 655 (2008)

M. Song, Z. Guo, M. Gao, C. Shi, D. Xu, L. You, et al., Synthesis and preliminary evaluation of a ^{99m}Tc-labeled folate-PAMAM dendrimer for FR imaging. Chem. Biol. Drug Des. **89**, 755 (2017)

A. Sulistio, J. Lowenthal, A. Blencowe, M.N. Bongiovanni, L. Ong, S.L. Gras, X. Zhang, G.G. Qiao, Folic acid conjugated amino acid-based star polymers for active targeting of cancer cells. Biomacromolecules **12**, 3469 (2011)

S.A. Torabizadeh, S.M. Abedi, Z. Noaparast, S.J. Hosseinimehr, Comparative assessment of a ^{99m}Tc labeled H1299.2-HYNIC peptide bearing two different co-ligands for tumor-targeted imaging. Bioorganic Med. Chem. **25**, 2583 (2017)

M.R. Vredenburg et al., Effects of orally active taxanes on P-glycoprotein modulation and colon and breast carcinoma drug resistance. J. Natl. Cancer Inst. **93**, 1234 (2001)

Y. Wang, B.B. Newell, J. Irudayaraj, Folic acid protected silver nanocarriers for targeted drug delivery. J. Biomed. Nanotechnol. **8**, 751 (2012)

M. Yousefi, A. Narmani, S.M. Jafari, Dendrimers as efficient nanocarriers for the protection and delivery of bioactive phytochemicals. *Adv. Colloid Interface Sci.* 102125 (2020)

H. Zheng, L. Yin, X. Zhang, H. Zhang, R. Hu, Y. Yin, T. Qiu, X. Xiong, Q. Wang, Redox sensitive shell and core crosslinked hyaluronic acid nanocarriers for tumor-targeted drug delivery. J. Biomed. Nanotechnol. **12**, 1641 (2016)